The anomalous behavior of the density of water in the range 30 K < *T* < 373 K

Francesco Mallamace*†‡, Caterina Branca*, Matteo Broccio*, Carmelo Corsaro*, Chung-Yuan Mou§, and Sow-Hsin Chen†

*Dipartimento di Fisica and CNISM, Università di Messina, C. da Papardo, S. ta Sperone 31, 98166 Messina, Italy; †Department of Nuclear Science and Engineering, Massachusetts Institute of Technology, Cambridge, MA 02139; and §Department of Chemistry, National Taiwan University, Taipei 106, Taiwan

Edited by H. Eugene Stanley, Boston University, Boston, MA, and approved September 27, 2007 (received for review July 11, 2007)

The temperature dependence of the density of water, $\rho(T)$, is obtained by means of optical scattering data, Raman and Fourier transform infrared, in a very wide temperature range, 30 < *T* < 373 K. This interval covers three regions: the thermodynamically stable liquid phase, the metastable supercooled phase, and the low-density amorphous solid phase, at very low *T*. From analyses of the profile of the OH stretching spectra, we determine the fractional weight of the two main spectral components characterized by two different local hydrogen bond structures. They are, as predicted by the liquid–liquid phase transition hypothesis of liquid water, the low- and the high-density liquid phases. We evaluate contributions to the density of these two phases and thus are able to calculate the absolute density of water as a function of *T*. We observe in $\rho(T)$ a complex thermal behavior characterized not only by the well known maximum in the stable liquid phase at *T* = 277 K, but also by a well defined minimum in the deeply supercooled region at 203 ± 5 K, in agreement with suggestions from molecular dynamics simulations.

infrared and Raman scattering | liquid–liquid phase transition | supercooled and amorphous water | Widom line in water

Understanding the fundamental role that water plays on Earth and in all aspects of life phenomena represents one of the most challenging research problems in science and technology. In comparison with other simple molecular liquids, the thermodynamic properties of water (H_2O) are characterized by a counterintuitive trend as temperature is lowered: examples are the isothermal compressibility, the isobaric heat capacity, the isobaric expansivity, and the density (1–3). The latter quantity, as is well known, exhibits a maximum at 277 K. Such a maximum is the only one occurring in liquids in their stable liquid phases just above the melting point. Over the years, many plausible explanations for these unusual behaviors have been proposed. In all of these explanations, the anomalies of water are invariably attributed to the role played by the hydrogen bond (HB) formation between water molecules (1). More precisely, the formation of HBs governs the overall structure and dynamics (1) of water, giving rise to, on decreasing *T*, a clustering process from which an open tetrahedrally coordinated HB network around each water molecule is gradually developed. It is such an increase in the HB structure that expands the liquid, compensating for the normal tendency of a liquid to contract as it is cooled. This finding is the basic reason for the occurrence of the density maximum phenomenon at 277 K (1–3).

Among the many theoretical approaches (4–6) developed to explain water properties in a supercooled state, there is the liquid–liquid phase transition (LLPT) hypothesis (6), which has received the most substantial support from various theoretical (7–10) and experimental studies (11, 12). For the LLPT model of water, the liquid state of water above the critical point is a mixture of two different local structures, characterized by different densities, namely, the low-density liquid (LDL) and the high-density liquid (HDL). In the HDL, the local tetrahedrally coordinated HB network is not fully developed, whereas in the LDL, a more open, locally "ice-like" HB network is fully realized (1–3). Water has within it regions that are locally more LDL-like and others that are locally more HDL-like (6–9). In addition, LDL and HDL correspond to the high-temperature continuation of the low- and high-density amorphous solid water phases, LDA (13) and HDA (14, 15), respectively. An important signature of the LLPT model is the prediction of a "second" critical point at $T_C \approx 220$ K and $P_C \approx 1$ kbar.

Actually, by means of molecular dynamics (MD) simulations (10) and spectroscopy experiments (16–18), we have some confirmations of the predictions of the LLPT theory. In these experiments, water was studied in the range $180 < T < 273$ K, inside a very deeply supercooled region and well below its nucleation temperature $T_H = 231$ K. In that case, to avoid crystallization, water was confined in nanostructures so narrow that the liquid could not freeze. From these experiments, by using both neutron scattering and NMR spectroscopy, a fragile-to-strong dynamic crossover (FSC) and the Stokes–Einstein relation violation (SEV) (17) at and below the crossover temperatures were observed (10), as confirmed in simulations (19). The FSC marks a transition from a Vogel–Fulcher–Tamman to an Arrhenius behavior in dynamical parameters (16). Both FSC and SEV take place at ambient pressure at about the same temperature, $T_L \approx 225$ K. Furthermore, on the P-T phase diagram, the observed FSC line coincides with the so-called Widom line (10, 12). The Widom line is the critical isochore above the LLPT critical point in the one-phase region. The neutron-scattering experiment located the end point of the Widom line, which is the predicted second critical point. In addition, Fourier transform infrared (FTIR) spectroscopy allows us to give direct evidence of the existence of the LDL phase in deeply supercooled, confined water (18). From this latter experiment, according to a well established procedure for the analysis of the OH stretching (OHS) vibrational mode, we have been able to measure the spectral contributions of the HB and non-hydrogen-bonded (NHB) water molecules, respectively, obtaining their relative concentrations. In addition, these FTIR data (18) point out that water evolves with continuity from the supercooled liquid into the LDA phase, as suggested by the liquid–liquid critical point theory.

Another important suggestion coming from the MD simulation studies, using both the TIP5P-E and the ST2 potential models for water, is that water exhibits a density minimum ≈70 K below the temperature of the density maximum (20, 21), T_M. Such a possibility may also be inferred from simple arguments on

Author contributions: F.M. and S.-H.C. designed research; F.M., C.B., M.B., and C.C. performed research; C.-Y.M. contributed new reagents/analytic tools; F.M., C.B., M.B., C.C., and S.-H.C. analyzed data; F.M., C.B., M.B., C.C., and S.-H.C. wrote the paper.

The authors declare no conflict of interest.

This article is a PNAS Direct Submission.

Abbreviations: FSC, fragile-to-strong dynamic crossover; FTIR, Fourier transform infrared; HB, hydrogen bond; LDA, low-density amorphous solid water phase; LDL, low-density liquid; LLPT, liquid–liquid phase transition; HDA, high-density amorphous solid water phase; HDL, high-density liquid; MD, molecular dynamics; NHB, non-hydrogen-bonded; OHS, OH stretching; PHB, partially HB; RTN, random tetrahedral network; SEV, Stokes–Einstein relation violation.

‡To whom correspondence should be addressed. E-mail: francesco.mallamace@unime.it.

considering the density data of supercooled bulk water, ice Ih, and LDA water (22). After the maximum, the density of bulk water decreases rapidly with decreasing T before T_H, whereas the ice Ih has a smaller density than that of the liquid and, contrary to supercooled bulk water, has a normal positive expansivity, that is, density increases as T decreases. The same behavior is observed for LDA at its highest temperatures. From the structural point of view, ice Ih represents the limiting case of a perfectly ordered tetrahedral network of HB, whereas LDA, which forms from deeply supercooled water, has a structure that very closely approaches that of a random tetrahedral network (RTN). Thus, ice Ih sets a lower bound for the density that the supercooled water could in principle attain. From these arguments, if the structure of deeply supercooled water approaches that of a RTN, and if nucleation can be avoided, it is then possible that a density minimum could occur in the deeply supercooled liquid.

Recently, the existence of a density minimum in the supercooled phase has been observed in confined D_2O by using neutron diffraction technique at the temperature $T_{min} = 210 \pm 5$K (23). Motivated by this result, we report here a study on the density of H_2O in a very wide temperature interval that includes LDA, supercooled confined water, and bulk water in the stable liquid phase. This study is done analyzing the spectra of the OHS vibrational modes obtained by means of Raman and FTIR spectroscopy. In particular, we have considered sound literature data of OHS Raman spectra of LDA (24) (in the range $30 < T < 130$ K) and of bulk water (25, 26) (in the range $250 < T < 373$ K), whereas for the T interval $183 < T < 303$ K we have considered the FTIR spectra of water confined in the same nanopores of the neutron diffraction experiment (18).

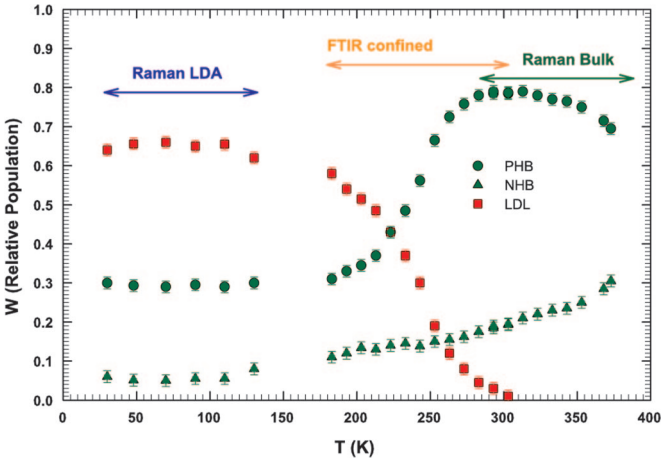

Fig. 1. The temperature dependence of the relative populations (W) of the three main spectral contributions to OHS vibrational bands of H_2O, obtained from Raman and FTIR spectroscopic experiments. PHB (green circles) and NHB (green triangles) refer to partially hydrogen-bonded and free water molecules, respectively. Fully tetrahedrally bonded molecules forming the RTN characterizing the LDL phase are reported as LDL (red squares). The different temperature regions where different experiments were performed are indicated. Raman data were taken in the two temperature ranges of low-density amorphous solid water (LDA; ref. 24) and bulk water in the thermodynamically stable liquid phase (25, 26, 29). FTIR data refer to confined water in the supercooled regime (18). The LDL phase shows up only below 303 K, whereas the other two phases exist over the entire studied temperature range. This latter result agrees with the fact that the water dynamics is not completely frozen even at $T = 30$ K, in agreement with experimental observations (30).

Experimental

Scattering methods have been largely used to study structural and dynamical properties of water and constitute the most used experimental approach to understand its properties. Indeed, neutron (11, 12), x-ray (27), and Raman and IR (25, 26, 28, 29) scattering, have given evidence that water is characterized by the presence of two coexisting main HB structural phases, involving HB and NHB molecules, respectively. Thus, it became customary to analyze OHS spectra by considering two general classes of O–H oscillators. These classes encompass broad Gaussian components, each referring to structures that involve a range of bond angles and distances distributed around the component peak position (29).

OHS spectra of water, as measured by Raman scattering and IR absorption in the range $30 < T < 647$ K (i.e., from the LDA phase to almost the first critical point of water), have been described by the following component Gaussian peak positions (wavenumbers) (29): (I) 3,120 cm^{-1}, (II) 3,220 cm^{-1}, (III) 3,400 cm^{-1}, (IV) 3,540 cm^{-1}, and (V) 3,620 cm^{-1} (within an experimental error of ± 20 cm^{-1}). All of them have been unambiguously classified as HB or NHB OHS oscillators by considering different scattering orientations (corresponding to the mean polarizability α and the anisotropy β) and, in particular, by their evolution as a function of temperature. The situation may be summarized as follows:

1. Component I dominates the intensity of the LDA phase (Raman data) (24), so that it represents the OHS contribution of water molecules forming the RTN. An analysis of its experimental FWHM in the T interval 30–303 K (i.e., in both the LDA and supercooled confined water) indicates that this can be identified as the LDL water phase (18). Its magnitude increases as T decreases.
2. Components II and III have been associated with water molecules having an average degree of connectivity larger than that of monomers, but lower than that involved in the HB networks. Thus, they can be identified as partially HB (PHB) (25, 26, 29) molecules.
3. Components IV and V, being the only ones present in the Raman and IR spectra of bulk water in the T region near the first critical point ($630 < T < 647$ K), arise from NHB monomeric water (or to molecules poorly connected to their environment) (25, 29). The integrated intensities of PHB and NHB water show an opposite temperature behavior for $T > 300$ K. While the intensities of NHB increase with increasing T, intensities of PHB decrease.

The classification of these contributions reflects that used in the percolation hypothesis for water (f_i species of water, with i indicating the number of bonds) (5). Thus, the HB component I is f_4, the NHB components IV and V are f_0, and, finally, the PHB components II and III are f_1, f_2, and f_3. We have to stress that according to the LLPT hypothesis, the HDL phase is represented by both the NHB and PHB. In Fig. 1 we report, in the interval $30 < T < 373$ K, the relative populations, W_{LDL}, of the LDL (red symbols) and W_{HDL} of the HDL (green symbols) water phases, calculated as the ratio of the component integrated area to the total OHS integrated area. For the latter phase, NHB (triangles) and PHB (circles) contributions are reported separately. According to the scattering theory, the relative populations are defined as $W_i = N_i/N$, where N_i and N are the number of the particles of the phase i and the total number of scattering particles, respectively. Data are collected from different experiments: for the temperature region 30–130 K, we used the data coming out from the analysis of Raman spectra of LDA (24); for $183 < T < 303$ K, we used our FTIR data on supercooled confined water (18); whereas for $253 < T < 373$ K, we analyzed Raman data of bulk water (25, 26, 29). It is apparent that the thermal behavior of all three species is continuous across the different temperature ranges, although coming from different data sets. As it can be observed, the NHB and PHB contributions are present at all temperatures, whereas the LDL phase exists

only in the range 30–303 K. The LDA phase is dominated by the LDL species, whereas in the stable liquid phase for $T > 303$ K, there is only the HDL. PHB population has a maximum at ≈303 K, decreases on decreasing T in the entire supercooled region, crosses LDL at ≈225 K, and finally becomes stable ($W \approx 0.29$) in the LDA phase.

From these results, it is evident that the HB RTN is formed essentially inside the metastable supercooled regime. It is also important to note that NHB and PHB are also present in the LDA phase. PHB is of the order of 30% and NHB is a few percent (≈6%) of the total water molecules, indicating that the dynamics of LDA is not completely frozen even at $T = 30$ K, in agreement with experimental observations (30).

Results and Discussion

Because only water contributes to the reported OHS spectra, its total density can be obtained only from the respective densities of its phases: the LDL and HDL. MD simulations (2) and proper neutron-scattering data give estimated values of the corresponding densities (11): $\rho_{HDL} \approx 1.2$ g/cm^3 and $\rho_{LDL} \approx 0.88$ g/cm^3. The density of LDA was experimentally measured (by decompression and warming to 120 K) as (31): $\rho_{LDA} \approx 0.94$ g/cm^3. According to these results, together with the experimental proof that the LDL phase exists only for $T < 303$ K (18), the HDL water is only given by the remaining spectral contributions classified as NHB and PHB.

Water density can be calculated knowing the fractioned populations of LDL and HDL (W_{LDL} and W_{HDL}) and their individual local densities, ρ_{LDL} and ρ_{HDL}. As shown in Fig. 1, W of different water species has an evident temperature dependence in all of the studied liquid regime (180–373 K). Also, the individual densities, because they are related to the local structure, may in principle change with temperature. The latter statement may be verified experimentally, considering, for instance, the region $T > 303$ K, where only the PHB and NHB species, whose populations were measured in bulk water, contribute to the OHS spectra (25). Thus, in the interval $303 < T < 373$ K, the densities ρ_{PHB} and ρ_{NHB} can be obtained from the bulk water density, according to the simple relation $\rho_{H_2O} = W_{PHB}\,\rho_{PHB} + W_{NHB}\,\rho_{NHB}$, where W represents the relative population of the two species (plotted in Fig. 1), at different temperatures within this interval. Because the density of bulk H_2O, ρ_{H_2O}, is well known from careful measurements in the range from 239 to 423K (32–35), by considering all of the W_{HDL} (W_{PHB} and W_{NHB}) data points measured in that T interval, we obtain the following values: $\rho_{PHB} \approx 1.10 \pm 0.02$ g/cm^3 and $\rho_{NHB} \approx 0.59 \pm 0.02$ g/cm^3. As a result, these values are temperature-independent within the reported experimental error. This finding is not surprising, considering the literature data on the proton magnetic resonance chemical shift of liquid water in a temperature range 273–363 K. This quantity, which, as is well known, entirely reflects the system local structure, does not exhibit any singularity or discontinuity in the temperature range above (36).

Two relevant situations emerge from our data analysis: (*i*) in the considered T range ($303 < T < 373$ K), the density depends on T only through W; (*ii*) $\rho_{NHB} \approx 0.59 \pm 0.02$ g/cm^3, according to Kell's representation (32, 33) of bulk water density as a function of T, corresponds to the density value at $T \approx 625$ K. Such a value is smaller than that used (0.66 g/cm^3 for $T = 673$ K, at a pressure of 800 bar) in a neutron-scattering experiment in the supercritical region, where no distinct HB peaks are observable in the O–H radial distribution function g_{OH} (37). Thus, the value of $\rho_{NHB} \approx 0.59 \pm 0.02$ g/cm^3 reasonably represents that of NHB water, which dominates Raman spectra in the region above the critical temperature. In addition, $\rho_{PHB} \approx 1.10 \pm 0.02$ g/cm^3 is comparable to the value proposed by neutron diffraction data for the HDL water ($\rho_{HDL} \approx 1.2$ g/cm^3; ref. 11). Therefore, the contribution of HDL to the total H_2O density, Δ_{HDL}, can be obtained in all of the explored T range ($30 < T < 373$ K), by extending the calculation made for ρ_{NHB} and ρ_{PHB} to the lowest temperatures. Fig. 2 *Inset* reports the results of this calculation (green data) as a function of T; as it can be observed, Δ_{HDL} increases with decreasing T in the range 310–373 K, then decreases continuously, with an inflection point at ≈250 K and finally, in the LDA phase, shows a slight decrease from ≈0.38 to an asymptotic value of 0.35 g/cm^3.

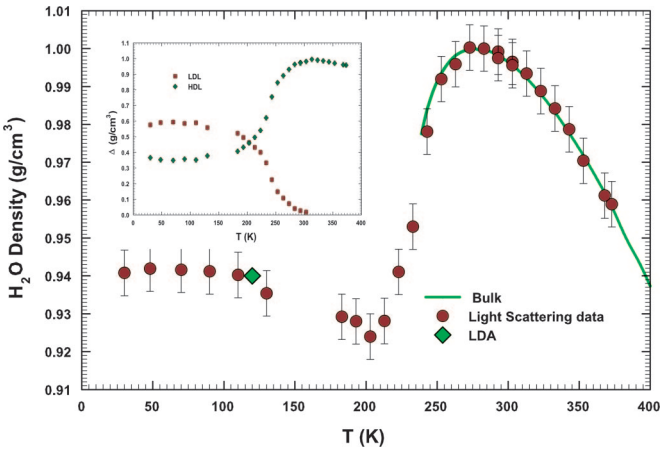

Fig. 2. The temperature dependence of calculated ρ_{H_2O}. The density values measured in pure bulk water in the range $239 < T < 423$ K (32–34) are reported as a solid line. As one can see, a minimum is evident at $T_M = 203 \pm 5$ K. For $T < T_M$ density smoothly rounds off to the constant value $\rho = 0.940 \pm 0.003$ g/cm^3 in the LDA phase. Inside this latter phase, by means of the method of decompression and warming, the density has been measured at 120 K, obtaining a value $\rho_{LDA} \approx 0.94$ g/cm^3, plotted as a green diamond (31). (*Inset*) The contribution Δ of the HDL (green diamonds) phase and LDL (red squares) phase to H_2O density as a function of temperature. The two Δ cross at ≈203 K. LDL and HDL are defined according to the LLPT hypothesis (6).

Analogously, the density contribution of the LDL phase, Δ_{LDL}, can be obtained by assuming that $\Delta_{LDL} = W_{LDL}\,\rho_{LDL}$. The ρ_{LDL} value can be calculated from $\rho_{H_2O} = \Delta_{HDL} + \Delta_{LDL} = \Delta_{HDL} + W_{LDL}\,\rho_{LDL}$. For this calculation we consider the temperatures 273 K and 28 3K (just around the density maximum, where W_{LDL} has been measured by Raman scattering in bulk water), where ρ_{H_2O} is 0.999868 and 0.99972 g/cm^3, respectively (as reported in ref. 32). In such a way we obtain $\rho_{LDL} = 0.87 \pm 0.02$ g/cm^3, a value that closely matches that proposed by neutron diffraction data analysis (11) for LDL water. Using such a value, we have obtained $\Delta_{LDL}(T)$ in all of the temperature intervals where LDL exists and reported it in Fig. 2 *Inset* as dark-red squares. As one can see, Δ_{LDL} increases with decreasing T and saturates to a value of ≈0.59 g/cm^3 on approaching the LDA temperature region. At the lowest T ($T < 100$ K), in the LDA phase, both Δ_{LDL} and Δ_{HDL} are nearly T-independent.

We report in Fig. 2 the temperature dependence of ρ_{H_2O} as the sum of the two contributions, Δ_{HDL} and Δ_{LDL}. For comparison, we also report the values measured in bulk water in the range $239 < T < 423$ K (32–34). As it can be observed, there is a good agreement between our density results and the literature data for ρ_{H_2O} in the supercooled regime (where, contrary to the range 273–373 K, data were not used to extract the values of ρ_{PHB}, ρ_{NHB}, and ρ_{LDL}). Two findings are remarkable: the minimum at ≈203 ± 5 K and the value of $\rho = 0.940 \pm 0.003$ g/cm^3 in the LDA phase, nearly the same as that measured in the LDA ice at $T =$ 120 K (31). This result, together with those obtained for $T >$303 K, confirms that the LDL and HDL local structures are essentially temperature-independent so the thermal evolution of water density comes only from that of W_{LDL} and W_{HDL}. Looking carefully at the data in the region of deep supercooling (≈250 K)

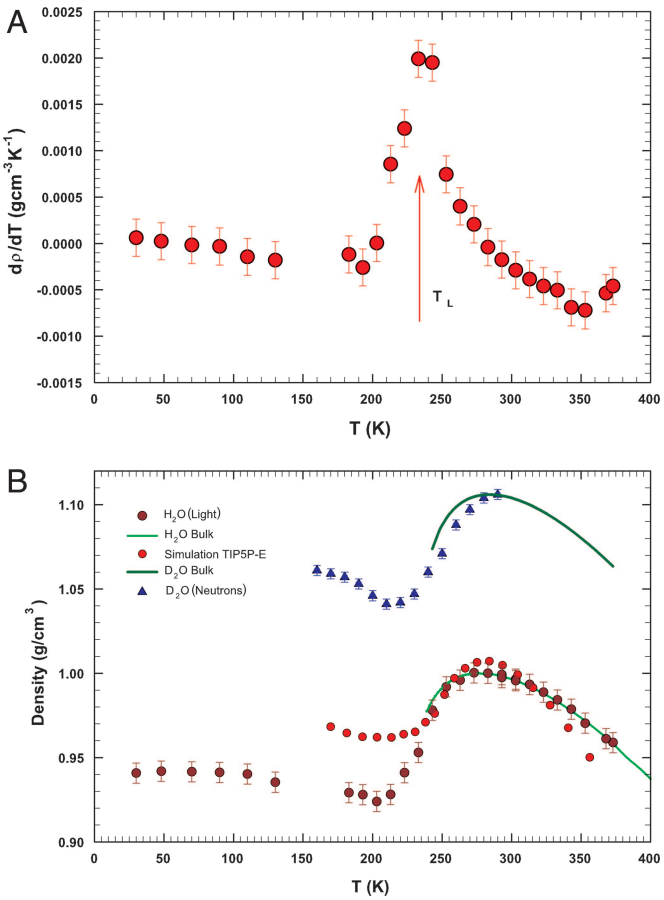

Fig. 3. Main properties of water density. (*A*) Derivative of ρ_{H_2O} with respect to temperature. The arrow indicates the Widom line temperature, T_L, at ambient pressure, that is, the locus of the correlation length maximum in the P–T plane. (*B*) Densities of H_2O (dark-red circles), D_2O, and that obtained for H_2O from MD simulation with the TIP5P-E potential (ref. 20; red circles) are reported. In the figure densities of D_2O measured in confined water by means of neutron scattering (ref. 23; blue triangles) and that of bulk heavy water (ref. 34; dark-green line) are reported. We also report the density data of bulk H_2O (light-green line; refs. 34 and 35). There is a good agreement between the experimental data of confined and bulk D_2O; these span about the same temperature range covered by MD simulation data. Instead, our density data cover a range including also the LDA temperature region. Between the density minima of H_2O and D_2O, there is the same temperature shift as that of their maxima (≈7 K); moreover, the difference between maximum and minimum (density amplitude) is about the same ($\rho \approx 0.08$ g/cm^3) for the two water isotopes.

it is possible to observe that our data, evaluated in confined water, are slightly lower than those measured in bulk. This finding may be attributed to the confinement effect of water inside the nanotubes, but the difference is not relevant enough to affect the overall result.

Besides the density minimum, an important result emerges from our experiment by estimating the derivative of the density with respect to temperature $(\partial\rho/\partial T)_P$, shown in Fig. 3*A*. As it can be observed, the inflection point between the maximum and the minimum in $\rho_{H_2O}(T)$ is located at temperature T_L corresponding to crossing of the Widom line at ambient pressure. Different phenomena have been correlated with the existence of the Widom line. Some examples are the SEV (17), a sharp change in the temperature derivative of the mean square displacement (12), and the maximum in the temperature derivative of the number of hydrogen bonds per molecule (18). We recall that SEV is due to the onset of dynamical heterogeneities whose typical length scale is a few water molecules size. Our finding, that is, the maximum in $(\partial\rho/\partial T)_P$, is thus not influenced by possible confinement effects and is closely linked to this latter result found in simulation. Here, we have described the temperature behavior of water density, in the supercooled regime, as mainly driven by the LDL phase. Thus, $(\partial\rho/\partial T)_P$ reflects the change of the local tetrahedral order with respect to temperature. In addition, it is of relevant interest, from a thermodynamic point of view, that the maximum in $(\partial\rho/\partial T)_P$ occurs at the same temperature as the Widom line: the temperature T_L is the locus of the correlation length maximum, whereas the density derivative is related with the cross-correlation between the entropy and volume fluctuations.

Fig. 3*B* reports the density of D_2O measured in the confined water by means of a small-angle neutron-scattering experiment (23) and, for comparison, the corresponding literature data of bulk heavy water (35). We also report the data for H_2O from the present experiment, which include the densities within the LDA phase, the densities in bulk (32–34), and the results of the quoted MD simulation of H_2O with the TIP5P-E potential (20). As one can see, there is a good agreement between the experimental data on H_2O and D_2O: their density minima have the same temperature shift as that of the corresponding maxima (≈7 K); moreover, the difference between maximum and minimum in the two cases are about the same ($\Delta\rho \approx 0.08$ g/cm^3). Although there is an observable difference between experimental densities of H_2O and MD simulations (20), this latter study still has the merit of suggesting and supporting the existence of a minimum in the water density. It is reasonably possible that, with the use of another water potential, MD simulation might give more reliable results than the experimental ones. We also need to highlight that the presented density data result "indirectly" from scattering experiments and may be susceptible of further improvements. Nevertheless, both experiments and simulations show unambiguously the existence of a minimum in the H_2O density in the deeply supercooled regime.

Methods

Raman data of LDA (24) and pure bulk water (25, 26) are reported in the literature. Samples of H_2O in the LDA phase have been obtained from vapor deposition on a sapphire substrate mounted on a cold finger. The corresponding OHS spectra have been measured with a double monochromator, excitating samples with an Ar laser source. For the pure bulk water, essentially the same experimental setup has been used. There are numerous data sets concerning this latter phase, which practically coincide regardless of the experimental setup used (25, 26, 29). For this work, we have used the data of refs. 25 and 26, which cover the range $249 < T < 373$ K. Refs. 24 and 25 provide the FWHM, the intensities (integrated areas), and the frequencies of the aforementioned Gaussian contributions, obtained by means of a best-fit procedure. In the case of ref. 26 spectra (measured by some of us), the data have been complemented with some new measurements and reanalyzed with the same customary procedure.

FTIR absorption measurements were performed as well at ambient pressure by confining water in a micelle-templated nanoporous silica matrix MCM-41-S (having 1D cylindrical tubes arranged in a hexagonal structure with a pore diameter of 1.4 nm) (38). As proven by several experimental methods, this MCM system can be regarded as one of the most suitable adsorbent models currently available (39, 40). In particular, it has been shown that in such a system water dynamics is weakly affected by confinement effects. By confining water, it is possible to probe liquid water at very low temperatures below its homogeneous nucleation temperature, T_H. In nanoscale confinement, the water molecules are unable to form a long-range crystalline structure.

The host material used in the FTIR experiments is the same as that used in neutron experiments, which were able to determine the density minimum of D_2O (23), having the same hydration level $h \approx 0.5$ (0.5 g of H_2O per gram of MCM). The experimental FTIR setup and the working procedure used are the same as described in ref. 18. In particular, our FTIR spectra of confined water were analyzed with the same deconvolution procedure as used for Raman data.

To calculate the density, we have considered the same approach used in ref. 23, based on the fundamental law of the scattering theory for which the integrated intensity of the scattered spectra $I(q,\omega)$ (where q is the scattering wavevector and ω is the frequency) is directly proportional to the number of the different species of scatterers. Namely, $I(q,\omega) = (N/V)P(q)S(q,\omega)$, where $P(q)$ is the scatterer form factor, $S(q,\omega)$ is the dynamic structure factor, whereas N denotes the number of scatterers in the scattering volume V. In the case of the neutron diffraction experiment of D_2O confined in MCM-41-S nanotubes, also the host material contributes to the scattered intensity $I(q)$, so that the heavy water density was obtained by assuming that the amplitude of the silica pores (temperature-independent in the studied T range) was an indicator of the density of water in the sample (23). In the case of the reported OHS spectra, only water contributes to them. Fig. 1 consists of the relative integrated areas, obtained from all of the aforementioned spectroscopic experiments, which cover separate temperature ranges characteristic of different water phases.

The research at Massachusetts Institute of Technolgoy is supported by a grant from the Materials Science Division of U.S. Department of Energy. The research at Università di Messina is supported by Messina University 2004. We benefited from affiliation with the EU Marie Curie Research and Training Network on Arrested Matter. We thank Professor Eugene H. Stanley for many fruitful discussions on the subject of water anomalies and the LL phase transition.

1. Angell CA (1982) in *Water: A Comprehensive Treatise*, ed Franks F (Plenum, New York), Vol 7, pp 1–81.
2. Debenedetti PG, Stanley HE (2003) *Phys Today* 56:40–46.
3. Mishima O, Stanley HE (1998) *Nature* 396:329–334.
4. Speedy RJ (1982) *J. Phys Chem* 86:982–991.
5. Stanley HE, Teixeira J (1980) *J Chem Phys* 73:3404–3422.
6. Poole PH, Sciortino F, Essmann U, Stanley HE (1992) *Nature* 360:324–328.
7. Moynihan CT (1997) *Mater Res Soc Symp Proc* 455:411–425.
8. Poole PH, Sciortino F, Grande T, Stanley HE, Angell CA (1994) *Phys Rev Lett* 73:1632–1635.
9. Borick SS, Debenedetti PG, Sastry SA (1995) *J Phys Chem* 99:3781–3793.
10. Xu LM, Kumar P, Buldyrev SV, Chen SH, Poole PH, Sciortino F, Stanley HE (2005) *Proc Natl Acad Sci USA* 102:16558–16562.
11. Soper AK, Ricci MA (2000) *Phys Rev Lett* 84:2881–2884.
12. Liu L, Chen SH, Faraone A, Yen CW, Mou CY (2005) *Phys Rev Lett* 95:117802.
13. Burton EF, Oliver WF (1936) *Proc R Soc Lond A* 153:166–172.
14. Mishima O, Calvert LD, Whalley E (1984) *Nature* 310:393–395.
15. Mishima O, Calvert LD, Whalley E (1985) *Nature* 314:76–78.
16. Mallamace F, Broccio M, Corsaro C, Faraone A, Wanderlingh U, Liu L, Mou CY, Chen SH (2006) *J Chem Phys* 124:161102.
17. Chen SH, Mallamace F, Mou CY, Broccio M, Corsaro C, Faraone A, Liu L (2006) *Proc Natl Acad Sci USA* 103:12974–12978.
18. Mallamace F, Broccio M, Corsaro C, Faraone A, Majolino D, Venuti V, Liu L, Mou CY, Chen SH (2007) *Proc Natl Acad Sci USA* 104:424–428.
19. Kumar P, Buldyrev S, Becker SR, Poole PH, Starr FW, Stanley HE (2007) *Proc Natl Acad Sci USA* 104:9575–9579.
20. Paschek D (2005) *Phys Rev Lett* 94:217802.
21. Poole PH, Saika-Voivoid I, Sciortino F (2005) *J Phys Condens Matter* 17:L431–L437.
22. Angell CA, Bressel RD, Memmati M, Sare EJ, Tucker JC (2000) *Phys Chem Chem Phys* 2:1559.
23. Liu D, Zhang Y, Chen CC, Mou CY, Poole PH, Chen SH (2007) *Proc Natl Acad Sci USA* 104:9570–9574.
24. Venkatesh CG, Rice SA, Bates JB (1975) *J Chem Phys* 63:1065–1071.
25. Walrafen GE (1967) *J Chem Phys* 47:114–126.
26. D' Arrigo G, Maisano G, Mallamace F, Migliardo P, Wanderlingh F (1985) *J Chem Phys* 75:4264–4270.
27. Bosio L, Chen SH, Teixeira J (1983) *Phys Rev A* 27:1468–1475.
28. Brubach J-B, Mermet A, Filabozzi A, Gerschel A, Roy P (2005) *J Chem Phys* 122:184509.
29. Walrafen GE (1974) in *Structure of Water and Aqueous Solutions*, ed Luck WAP (Verlag Chemie, Weinheim, Germany), pp 248–284.
30. Smith RS, Huang C, Kay BD (1997) *J Phys Chem B* 101:6123–6126.
31. Floriano MA, Handa YP, Klug DD, Whalley E (1989) *J Chem Phys* 91:7187–7192.
32. Kell GS (1967) *J Chem Eng Data* 12:66–69.
33. Kell GS (1975) *J Chem Eng Data* 20:97–105.
34. Sorensen CM (1983) *J Chem Phys* 79:1455–1461.
35. Vedamuthu M, Singh S, Robinson GW (1996) *J Phys Chem* 100:3825–3827.
36. Modig K, Pfrommer B, Halle B (2003) *Phys Rev Lett* 90:075502.
37. Soper AK, Bruni F, Ricci MA (1997) *J Chem Phys* 106:247–254.
38. Shih PC, Lin HP, Mou CY (2003) *Stud Surf Sci Catal* 146:557–560.
39. Schreiber A, Ketelsen I, Findenegg GH (2001) *Phys Chem Chem Phys* 3:1185–1195.
40. Morishige K, Nobuoka K (1997) *J Chem Phys* 107:6965–6969.